XVI International Conference on Durability of Building Materials and Components
DBMC 2023, China
K.F. Li and D.P. Fang (Eds)

Investigation of the Initial Quality of Robotic Tile Installation Based on Coupled Eulerian-Lagrangian Approach

K. Wu[1], Y.R. Zhang[1], X.M. Kong[2] and S. Zhang[1]

[1]School of Civil Engineering, Beijing Jiaotong University, Beijing 100044, PR China,
20115060@bjtu.edu.cn (First K. Wu), yr.zhang@bjtu.edu.cn (Corresponding author),
21121218@bjtu.edu.cn (Fourth S. Zhang)

[2]Department of Civil Engineering, Tsinghua University, Beijing 100084, PR China,
kxm@mail.tsinghua.edu.cn (Third X.M. Kong)

Abstract. *In this study, the initial quality of robotic tile installation under various construction parameters and material properties of adhesive were investigated based on the fluid–structure coupling construction models for the first time. First, the models of adhesive application and tile leveling were developed based on the coupled Eulerian–Lagrangian approach. Then, on the basis of these models, various patterns of adhesive application, types of tile leveling loads, numbers of adhesive strips and yield stresses of adhesive were simulated and their influence laws on the initial quality of robotic tile installation were analyzed. Finally, the influence mechanisms of these parameters on the installation quality were revealed in terms of the spacing between adhesive strips, tile rebounding, contact areas and defect distribution. Results showed that the adhesive with horizontal application possessed smaller plastic deformation, kept stable shape of strips and distributed at equal spacing, compared with the one with vertical application. In contrast to a single compression load, its couplings with vibration loads were beneficial to the reduction of tile rebounding. Among the coupling loads, the coupling of shear vibration with compression considerably increased the tile–adhesive contact area until no interfacial defect appeared. The increase of the number of adhesive strips exerts few effects on the installation quality, including slight increases of contact areas as well as diminished interfacial defects. In the case of relatively low and high yield stresses of adhesive, the shear vibration effects were respectively large and small which decrease the installation quality.*

Keywords: *Robotic tile installation; Construction parameters; Material property; Initial quality; Fluid-structure coupling*

1 Introduction

Robots have been increasingly used in various field of construction industry to accelerate the transformation from traditional human labor to automation and intelligence [1]. The replacement of robots for human performs the tedious, repetitive, and high-intensity work, improving the production efficiency and achieving semi-automated or automated operation. Tile installation is a simple and repeat task, and thus has become one of the most suitable parts of construction engineering for the robotic application [2]. The use of tile installation robots (as shown in Figure 1) effectively solves the problem of labor shortage, reduces construction costs, improves construction quality, and contributes to the sustainable development of construction industry.

(a) Adhesive application (b) Tile leveling

Figure 1. Mobile Robotic Tiling [3].

Extensive research has been carried out to design the robots for tile installation [4-10], aiming at the function enhancement and integrated design of different modules in the robots. Apostolopoulos et al. [4] proposed a floor-tile installation robot with omni-directional locomotive capability, which is equipped with a laser-based triangulation system for navigation and positioning and a high-resolution camera for the evaluation of installation quality. Navon et al. [5] utilized a graphic simulation system to test a floor-tilling robot with six DOF arm, and developed a computer vision system for tile installation with high-precision and defect detection. Liu et al. [6] designed a tiling robotic system which employed a sensor system for the detection of the conditions of walls and ground and the precise control of the adhesive thickness and tile placement, and achieved the installation of 150 mm × 150 mm tiles in 10 seconds. Liu et al. [7] developed a track motion tiling robot that integrated illumination-independent spatial positioning technology and smooth placement pattern of multi-segment path planning, and reduced working time by 20.9% compared to human labor. Li et al. [8] proposed a new adaptive vision-based control scheme for robotic tiling, which enabled the automatic tile picking in the presence of uncalibrated cameras and limited field of view, significantly enhancing the autonomy of tiling robots. Wang et al [9] introduced an algorithm for complementing tile position information based on visual measurement, and evaluated the quality of tile laying online. Xu et al [10] presented an automatic ceramic tile applicator which continuously completed the mixing and application of cement slurry, saving nearly 50% of time and reducing the hollowing rate to 0.1% during construction. However, so far, little literature is available concerning the effects of construction parameters of robots and material property of adhesive on the quality of tile installation.

In this study, fluid–structure coupling construction models of a tile–adhesive–concrete system were developed, and the influence laws and mechanisms of various intelligent construction parameters and material property of adhesive on the initial quality of robotic tile installation were investigated for the first time. First, the models of adhesive application and tile leveling were established based on the coupled Eulerian–Lagrangian approach and their rationality was verified. Then, various patterns of adhesive application, types of tile leveling loads, numbers of adhesive strips and yield stresses of adhesive were simulated, and their influence laws on the initial quality of tile installation were analyzed. Indices of the spacing between adhesive strips, tile rebounding, contact areas and defect distributions were adopted to characterize the installation quality of tile. Finally, the influence mechanisms of intelligent construction parameters and material property of adhesive on the installation quality of ceramic tiles were revealed. This study is expected to provide a theoretical guidance for the optimization of construction process of a robot for tile installation, and to promote the application of intelligent construction technology and the high-quality development of construction industry.

2 Coupled Eulerian–Lagrangian approach (CEL)

In continuum mechanics, Lagrangian formulation and Eulerian formulation are two fundamental algorithms in analysis of continuous media. The former possesses an accurate description of object boundary but encounters the mesh distortions with simulation of large deformation. The latter deals with the problems of extreme deformation but is incapable of accurately capturing the object boundary [11]. Therefore, the Lagrangian formulation is commonly used in solid mechanics while the Eulerian formulation is adopted in fluid mechanics.

In 1964, Noh [11] first proposed the CEL approach, which combines the advantages of both formulations and thus is suitable for the simulation of complex fluid-structure coupling structures. Lagrangian formulation and Eulerian formulation both follow the laws of mass, momentum and energy conservation. The former uses the material time derivative and the latter uses the spatial time derivative in the conservative equations, as shown in Table 1 [12]. In addition, the Eulerian equations have the general conservation form as Eq. (1). The CEL approach divides this equation into Eq. (2) and Eq. (3), corresponding to the Lagrangian step and the Eulerian step, and solves them in sequence.

Table 1. Conservative equations [12].

Conservative equations	Relation between the material and spatial time derivatives	Lagrangian formulation	Eulerian formulation
Mass		$\frac{\mathrm{D}\rho}{\mathrm{D}t}+\rho\nabla\cdot\boldsymbol{v}=0$	$\frac{\partial\rho}{\partial t}+\nabla\cdot(\rho\boldsymbol{v})=0$
Momentum	$\frac{\mathrm{D}\phi}{\mathrm{D}t}=\frac{\partial\phi}{\partial t}+\boldsymbol{v}\cdot(\nabla\phi)$	$\rho\frac{\mathrm{D}\boldsymbol{v}}{\mathrm{D}t}=\nabla\cdot\boldsymbol{\sigma}+\rho\boldsymbol{b}$	$\frac{\partial\rho\boldsymbol{v}}{\partial t}+\nabla\cdot(\rho\boldsymbol{v}\otimes\boldsymbol{v})=\nabla\cdot\boldsymbol{\sigma}+\rho\boldsymbol{b}$
Energy		$\frac{\mathrm{D}e}{\mathrm{D}t}=\boldsymbol{\sigma}:\boldsymbol{D}$	$\frac{\partial e}{\partial t}+\nabla\cdot(e\boldsymbol{v})=\boldsymbol{\sigma}:\boldsymbol{D}$

Note: $\frac{\mathrm{D}}{\mathrm{Dt}}$ is the material derivative, $\frac{\partial}{\partial t}$ is the spatial time derivative, ϕ is the arbitrary solution variable, $\boldsymbol{v}\cdot\nabla$ is the convective term, $\boldsymbol{v}$ is the material velocity, ∇ is the gradient operator, ρ is the density, $\boldsymbol{\sigma}$ is the Cauchy stress, $\boldsymbol{b}$ is the body force, e is the internal energy per unit volume, $\boldsymbol{D}$ is the strain rate.

$$\frac{\partial\phi}{\partial t}+\nabla\cdot\boldsymbol{\Phi}=\boldsymbol{S} \tag{1}$$

$$\frac{\partial\phi}{\partial t}=\boldsymbol{S} \tag{2}$$

$$\frac{\partial\phi}{\partial t}+\nabla\cdot\boldsymbol{\Phi}=0 \tag{3}$$

where ϕ is the arbitrary solution variable, $\boldsymbol{\Phi}$ is the flux function and $\boldsymbol{S}$ is the source term.

3 Development of the numerical model

3.1 Experiment of the yield deformation of tile adhesive

Figure 2 shows the experiment of the yield deformation of tile adhesive. The procedure of experiment is as follows: 1) A cylindrical mold with a diameter of 60 mm and a height of 20 mm was placed in the center of a wet glass plate (200 mm × 200 mm × 15 mm). 2) Well-mixed adhesive of Davco TTB I type (water to adhesive ratio of 6:25) was poured into the cylindrical mold and flatten at the top. 3) The cylindrical mold was lifted vertically and steadily. 4) A glass plate weighing 0.2 N was placed on the top of adhesive which kept stable. 5) A load of 2 N was applied to the glass plate, and the final diameter of adhesive at the bottom was recorded after it stopped deforming. Similarly, the final diameters of adhesive at the bottom were recorded when the loads were 4 N and 6 N.

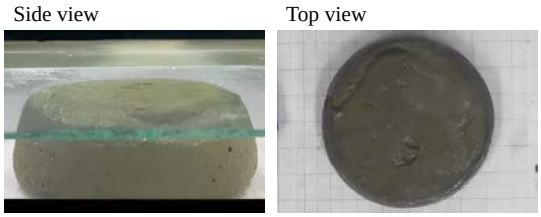

Figure 2. Experiment of the yield deformation of tile adhesive.

3.2 Simulation of the yield deformation of tile adhesive

The numerical model of the yield deformation of tile adhesive was established as shown in Figure 3. From top to bottom, there are the top glass plate, the adhesive, and the bottom glass plate in the model. The glass plates were modeled as rigid bodies. The adhesive was simulated in the Eulerian domain with the constitutive equation of Drucker-Prager model. The related physical and mechanical parameters are shown in Table 2. Loading 2 N, 4 N, and 6 N on the top glass plate, the corresponding final diameters of the tile adhesive at the bottom were calculated.

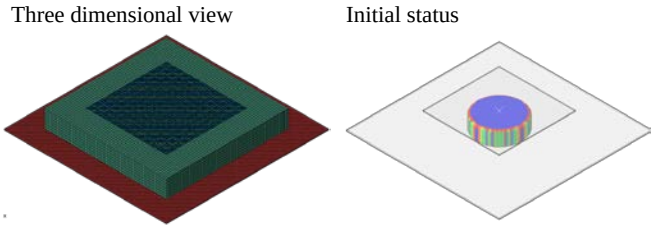

Figure 3. Model of the yield deformation of tile adhesive.

Table 2. Physical and mechanical parameters of tile adhesive.

Density/(kg/m^3)	Elastic modulus/Pa	Poisson ratio	Friction angle/°	Flow stress ratio	Dilation angle/°	Yield Stress/Pa
2200	193700	0.49	0	1	0	300

Figure 4 exhibits the comparison of adhesive diameter between numerical and experimental results. It can be seen that the numerical result varies consistently with the experimental result, and their maximum difference is only −1.98%. This indicates the reasonableness of the constitutive model and material parameters of the adhesive.

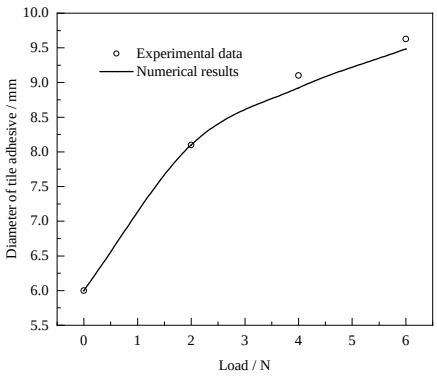

Figure 4. Comparison between numerical and experimental results.

3.3 Fluid-structure coupling model of tile-adhesive-concrete

Referring to the mobile robotic tiling shown in Figure 1, the construction models of tile-adhesive-concrete based on CEL approach were established, including the model of adhesive application (Figure 5 (a)) and the model of tile leveling (Figure 5 (b)). The former consists of Eulerian domain and concrete, and was used to analyze the influence of the pattern of adhesive application on the deformation of adhesive. The latter consists of tile, Eulerian domain and concrete, and was utilized to analyze the influences of the tile leveling loads, number of adhesive strips and yield stress of adhesive on the indices of tile rebounding, contact areas, defect distribution, etc.

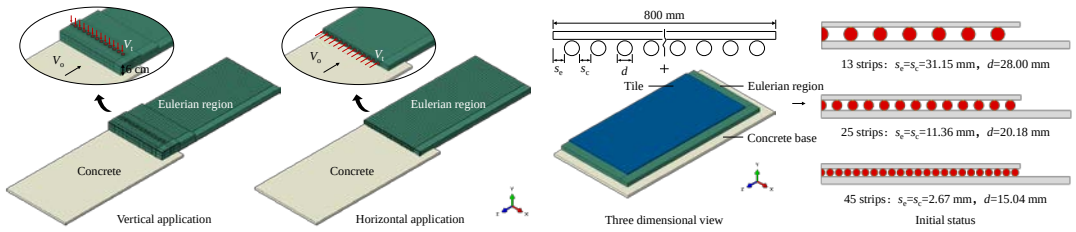

(a) Model of adhesive application (b) Model of tile leveling

Figure 5. CEL construction models of tile–adhesive–concrete. V_o is the moving speed of the outlets of adhesive extrusion, V_t is the speed of adhesive extrusion, s_e is the distance from the outer outlet of adhesive extrusion to the edge of tile, s_c is the spacing of the outlets of adhesive extrusion, d is the diameter of the outlet of adhesive extrusion.

In the construction models, the sizes of the tile and concrete are 0.8 m × 0.8 m × 0.01 m and 1.0 m × 1.0 m × 0.015 m, respectively. The design volume of adhesive was selected as 0.0064 m^3 (0.8 m × 0.8 m × 0.01 m) and substituted to Eq. (4) to calculate the sizes of outlets of adhesive extrusion. With reference to one tile, the length of adhesive in the model of adhesive application is 0.8 m. Since the robotic application of adhesive is consecutive, the length of

adhesive in the model of tile leveling was taken as 0.9 m, considering the effects of adhesive applied out of the tile. The size of the Eulerian domain meets the requirement of containing the whole deformation region of adhesive. The tile and concrete were both modeled as rigid bodies and represented by 110,000 and 170,000 solid elements, respectively. The adhesive was modeled as a Eulerian part with 2.5 million (application model) and 5.9 million (leveling model) Eulerian elements. "Hard" and "Penalty" contacts (with a friction coefficient of 1) were used for the normal and shear interactions between the adhesive and the tile, and between the adhesive and the concrete. The density of the tile and concrete is 2400 kg/m^3 and 2300 kg/m^3, and the material parameters of adhesive are shown in Table 2.

$$\begin{cases} 0.8 \times \dfrac{n\pi d^2}{4} = V \\ nd + (n-1)s_c + 2s_e = 0.8 \end{cases} \tag{4}$$

where n is the number of adhesive strips and V is the design volume of adhesive.

In the model of adhesive application, the number of adhesive strips is 25, as presented in Figure 5 (a). The speed of adhesive extrusion and moving speed of the outlets of adhesive extrusion are 0.25 m/s but in opposite directions. A velocity condition was set to the concrete to simulate the movement of the outlets of adhesive extrusion. In the model of tile leveling, the numbers of adhesive strips are 13, 25, 45 as exhibited in Figure 5 (b). The concrete was fixed and symmetrical constraints were set at both ends of the adhesive in the longitudinal direction. The tile bears three types of leveling loads (Figure 6) after compression loads. The compression loads pressed the adhesive to be with thickness of 10 mm within 2 s. The leveling loads include compression (holding the adhesive thickness of 10 mm, lasting for 5 s), vertical vibration with compression (0.025 mm, 50 Hz, lasting for 5 s) and shear vibration with compression (0.025 mm, 50 Hz, lasting for 5 s). To improve computational efficiency, the abovementioned models are half models, and symmetrical constraints were set on the symmetrical surface. Gravity load was applied to all models during calculation.

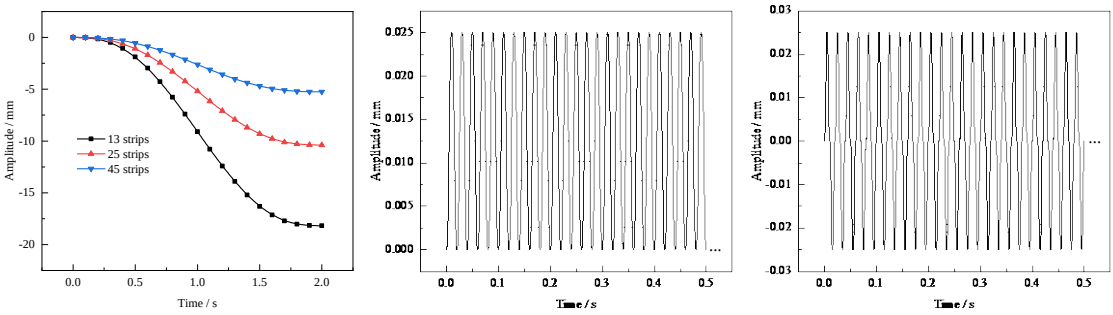

(a) Compression (b) Vertical vibration (c) Shear vibration

Figure 6. Amplitude curves of loads.

4 Results and discussion

4.1 Effect of the pattern of adhesive application

Figure 7 shows the contour plots of the equivalent plastic strains of tile adhesive applied

horizontally and vertically. It can be seen clearly that the tile adhesive with vertical application bends after contacting the concrete and has equivalent plastic strains up to 4.16. Hence, the shape of tile adhesive strips undergoes a significant change, with many of them collapsing into a semi-cylindrical shape and with the spacing between them decreasing. In contrast, the equivalent plastic strains of tile adhesive with horizontal application are lower than 0.56, indicating small plastic deformation. This results in the tile adhesive almost maintaining a stable quasi-cylindrical shape and distributing at equal spacing.

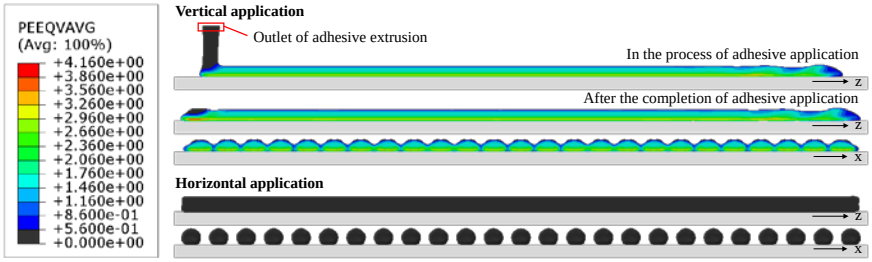

Figure 7. Contour plots of the equivalent plastic strains of tile adhesive applied horizontally and vertically. z: the direction of adhesive application; x: perpendicular to the direction of adhesive application.

In the process of adhesive application, the plastic deformation of adhesive mainly depends on the yield stress, friction, gravity, etc. With vertical application, the adhesive initially produces small equivalent plastic strains lower than 0.56 under the action of gravity. Then, the kinetic energy of adhesive converts into plastic deformation energy after the adhesive contacts with substrate, leading to a significant change in the shape of adhesive. When the adhesive is applied horizontally, the gravity force of adhesive is balanced by the support force of substrate. The moving speed of extrusion outlets is equal in magnitude but opposite in direction to the speed of adhesive extrusion, ensuring that the adhesive and the substrate remain relatively stationary. This causes tiny friction from the substrate which is insufficient to cause yield deformation of the adhesive. Therefore, the adhesive basically maintains its original shape throughout the entire process of horizontal application.

4.2 Effect of the type of tile leveling loads

(1) Vertical displacements and forces

Figure 8 shows the effects of the type of tile leveling loads on the vertical displacements D_v and vertical forces F_v of tile. In the figure, the negative displacement indicates downward movement of the ceramic tile, the positive and negative forces respectively represent the pulling and pressing of tile. In the stage of tile pressing, the displacement D_v increases to the target displacement D_t within 2 s, which is in accordance with the loading mode of tile pressing shown in Figure 6. Correspondingly, the force F_v turns from pulling force to pressing force, and the pressing force increases to the maximum value F_m in the end.

During the stage of tile leveling, the displacement D_v keeps constant under the action of compression, and the force F_v decreases slightly. When loading the vertical vibration, the displacement D_v fluctuates in an amplitude of 0.025 mm, and the force F_v decreases continuously with a sync fluctuation. Under the action of shear vibration, the displacement D_v

stays stable, the force F_v firstly decreases and then increases after a transition from pressing force to pulling force (6.0 s).

After the removal of compression and vertical vibration, the displacements D_v present an increase before stabilization, and the forces F_v respectively exhibit an instant drop from 2.72 kN and 1.72 kN to zero. However, the displacement D_v keeps stable after the removal of shear vibration, and the force F_v drops from 0.033 kN to zero immediately.

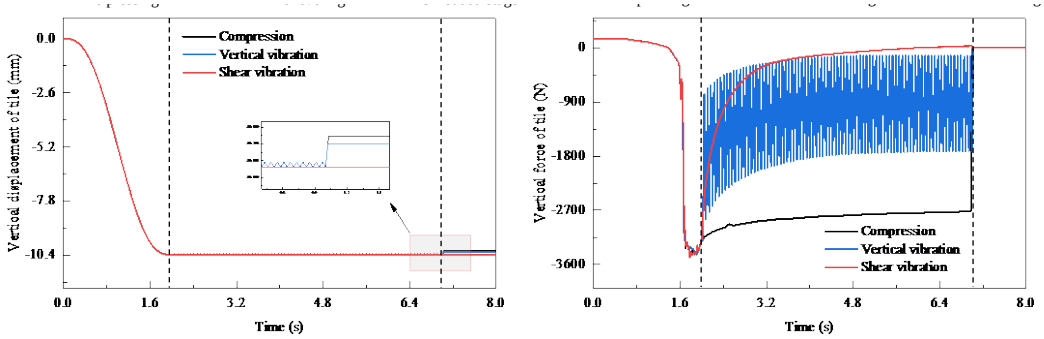

(a)Vertical displacements (b)Vertical forces

Figure 8. Variations of the vertical displacements and vertical forces of tile with time under various types of tile leveling loads.

As is well known, the adhesive produces elastic deformation and plastic deformation during the process of tile pressing. The elastic deformation of adhesive generates a rebounding force on the bottom of tile, which equals to the sum of gravity and vertical force F_v of tile. At the initial moment of tile pressing, the rebounding force is zero, and the force F_v is a pulling force to balance the gravity of tile (150 N). As the vertical displacement D_v of tile rises, the compression deformation of adhesive increases, and the rebounding force accordingly becomes larger. This leads to a transition of F_v from pulling force to pressing force and then a continuously increasing pressing force.

During the leveling stage, the adhesive gradually stabilizes under the action of compression with constant amplitude. The deformation of adhesive increases slightly, resulting in a slight decrease of F_v. In terms of the vibration loadings, the plastic deformation of adhesive increases with longer loading time. This causes a decreasing proportion of elastic deformation and an accordingly gradual reduction of rebounding force. Hence, the forces F_v decrease under the action of vertical vibration and shear vibration. Moreover, the shear vibration remarkably increases the plastic deformation of adhesive, which reduces the value of rebounding force to be lower than the one of tile gravity. This leads to the transition from pressing force to pulling force.

After removal of the leveling loads, all the forces F_v become zero. In terms of the compression and vertical vibration, the rebounding forces of adhesive cause the tile rebounding with a recovery of the elastic deformation of adhesive. However, in the circumstance of shear vibration, the adhesive is hard to produce plastic deformation under the action of tile gravity. Thus, the displacement D_v remains almost unchanged.

(2) Contact areas

Figure 9 exhibits the effects of type of tile leveling loads on the tile–adhesive contact area

S_1 and adhesive–concrete contact area S_2. In the stage of tile pressing, the contact area S_1 increases from zero to the maximum value $S_{1,\,max}$ of 0.64 m^2, and the contact area S_2 increases from 0.34 m^2 to the maximum value $S_{2,\,max}$ of 0.64 m^2.

During the stage of tile leveling, the contact areas S_1 and S_2 remain a stable value of 0.64 m^2 under the action of compression. When loading the vertical vibration and shear vibration, the contact area S_1 decreases in a fluctuating pattern, and the contact area S_2 keeps 0.64 m^2. In the unloaded stage, the removal of compression leads to the decreases of contact areas S_1 and S_2 to the values of 0.265 m^2 and 0.632 m^2. After canceling the vertical vibration, the contact area S_1 reduces to 0.240 m^2 and the contact area S_2 remains 0.64 m^2. In contrast, the contact areas S_1 and S_2 keep stable at 0.625 m^2 and 0.64 m^2 after the cancellation of shear vibration.

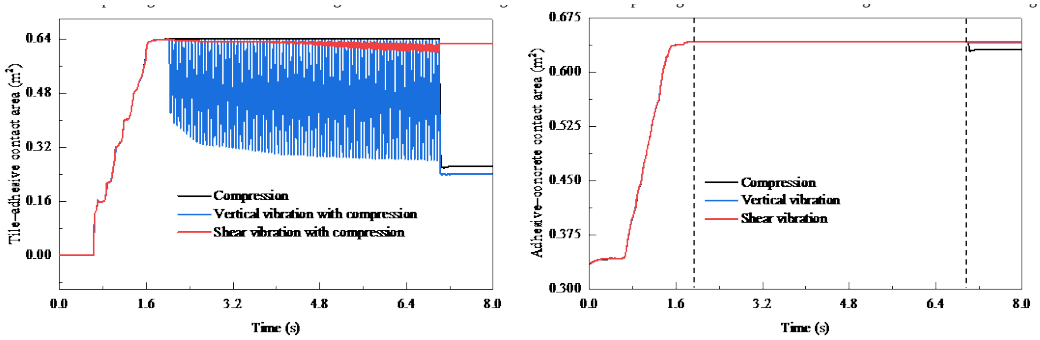

(a) Tile–adhesive contact area S_1 (b) Adhesive–concrete contact area S_2

Figure 9. Variations of the tile–adhesive contact area and adhesive–concrete contact area with time under various types of tile leveling loads.

The variations of contact areas mainly depend on the initial status of adhesive and the deformation of adhesive during the loading process. At the initial moment of tile pressing, the adhesive is not in contact with the tile, leading to a contact area S_1 of zero. On the contrary, the adhesive is in contact with the concrete, leading to a contact area S_2 of 0.34 m^2. During the process of tile pressing, the adhesive deformation gradually increases, and contact areas both rise to the maximum value.

In the stage of tile leveling, the compression keeps the tile stationary and thus constant contact areas. When subjected to the vertical vibration, the upward and downward movements of tile cause the decrease and increase of contact area S_1. With increasing time of vertical vibration loading, the plastic deformation of adhesive increases, whose increasing amount is especially large at the low-constrained rim of tile. This results in the adhesive presenting a full state in the middle and a collapsed state at the rim, which decreases the contact area S_1 when the tile moves upward. The vertical vibration possesses a small amplitude of 0.025 mm and has little effect on the contact area S_2. Under the action of shear vibration, the forward and backward shear movements of tile cause the decrease and increase of contact area S_1. As the loading time of shear vibration increases, the adhesive produces larger plastic deformation while the tile keeps the same position in the vertical direction. This causes more adhesive to detach from the tile, which decreases the contact area S_1 accordingly. The shear vibration acts at the tile-adhesive interface and has little effect on the contact area S_2.

In the unloaded stage, the elastic deformation of adhesive recovers after the removal of

compression, decreasing the contact areas S_1 and S_2. After the cancellation of vertical vibration, the contact area S_1 decreases due to the recovery of elastic deformation of adhesive, while the contact area S_2 keeps constant due to the uniform deformation of adhesive at the adhesive-concrete interface. In contrast, the adhesive subjected to shear vibration has little rebounding deformation, ensuring the uniform deformation of adhesive. Thus, the contact areas S_1 and S_2 remain stable after removing the shear vibration.

(3) Initial installation quality

The effects of loading type on the initial installation quality of ceramic tiles are shown in Figure 10. Compared with single compression, its coupling with vertical vibration respectively reduces the tile rebounding and contact area S_1 by 27.33% and 9.43% and slightly increases the contact area S_2 by 1.27%. In contrast, the coupling of shear vibration with compression eliminates the tile rebounding, and respectively increases the contact area S_1 and S_2 by 100% and 135.85%. This indicates that the vibration loads reduce the value of tile rebounding effectively, which is beneficial to the initial surface flatness of tile. However, the vertical vibration triggers uneven deformation of the adhesive and further reduces the contact area S_1. In contrast, the contact area S_1 increases remarkably under the action of shear vibration with compression. This is mainly due to the fact that the adhesive produces uniform plastic deformation during the loading process of shear vibration and possesses zero rebounding deformation after the removal of loading.

In addition, the tile-adhesive and adhesive-concrete interfacial defects appear at the rim of tile under the action of compression. Compared with the compression, the coupling of vertical vibration with compression leads to an increasing tile-adhesive interfacial defect which is more concentrated at the rim of tile. The presence of these defects in a large tiling system significantly accelerates the further development of tile detachment after the hardening of adhesive. In contrast, few detachment strips distribute uniformly at the tile-adhesive interface and no detachment appears at the adhesive-concrete interface under the action of shear vibration with compression. This proves full contacts of the adhesive with the tile and with the concrete, meaning the best installation quality.

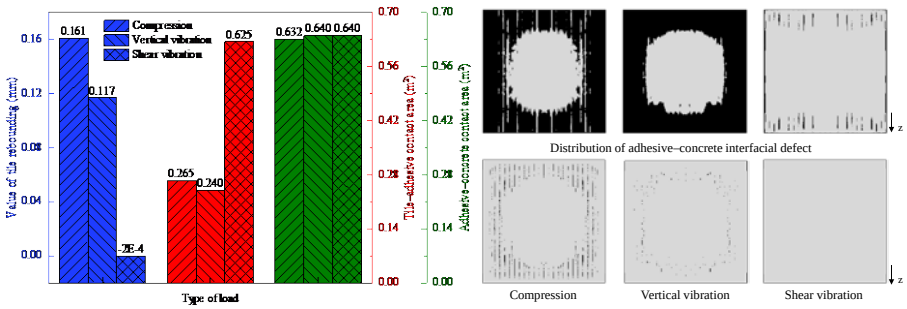

Figure 10. Initial installation quality of ceramic tiles under the actions of various loads. Black in the contour plots of interfacial defect: interfacial defect caused by detachment of tile adhesive.

4.3 Effect of the number of adhesive strips

(1) Vertical displacements and forces

The effects of the number of adhesive strips on the vertical displacements D_v and vertical

forces F_v of tile are exhibited in Figure 11. In the stage of tile pressing, the displacement D_v and force F_v increase faster with increasing adhesive strips. In the stage of tile leveling, the displacements D_v all keep stable under various adhesive strips, and the force F_v presents a slightly faster decrease with the increase of adhesive strips. After the removal of shear vibration, the displacement D_v under 13 strips increases by 9×10^{-4} mm, and the force F_v under 13 strips decreases from a pressing force of 0.018 kN to zero. On the contrary, the displacements D_v under 25 and 45 strips respectively decrease by -2×10^{-4} mm and -3×10^{-4} mm, and the forces F_v under 25 and 45 strips respectively decrease from pulling forces of 0.035 kN and 0.045 kN to zero.

In the stage of tile pressing, the displacements D_v vary according to the loading mode of Figure 6. As shown in Figure 5, increasing adhesive strips lead to narrower spacing between them. This means more adhesive contacted with the tile and the earlier contact between adhesive strips, thereby accelerating the increase of force F_v. As mentioned in section 4.2, the shear vibration increases the plastic deformation of adhesive, and thus decreases the rebounding force and the force F_v. With the increase of adhesive strips, the shear vibration has a bit more effects on the plastic deformation of adhesive. This causes a slightly faster decrease of the force F_v. With respect to 13 strips, the rebounding force from adhesive after shear vibration is larger than the tile gravity. Hence, the tile rebounds and force F_v decreases from a pressing force to zero. Oppositely, the rebounding force from adhesive after shear vibration is smaller than the tile gravity under 25 and 45 strips, which brings about the sinking of tile and the decreases of forces F_v from pulling forces to zero.

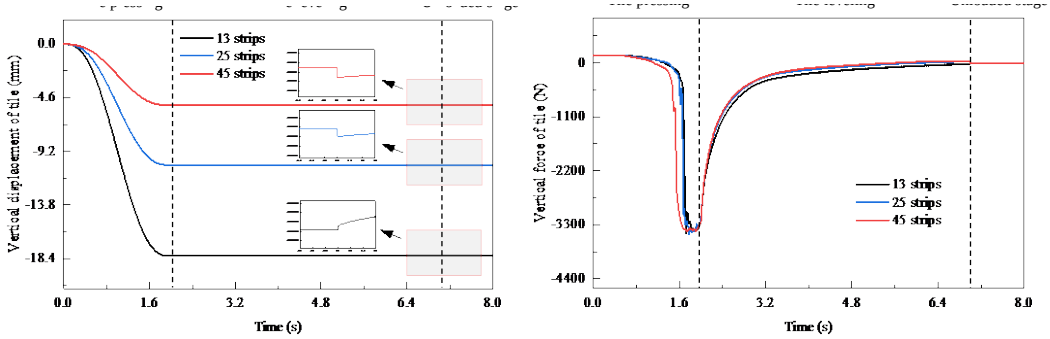

(a) Vertical displacement of tile (b) Vertical force of tile

Figure 11. Variations of the vertical displacements and vertical forces of tile with time under various number of adhesive strips.

(2) Contact areas

Figure 12 shows the contact area S_1 and contact area S_2 under various adhesive strips. In the stage of tile pressing, the contact areas S_1 and S_2 present earlier rises and larger $S_{1,\,max}$ and $S_{2,\,max}$ with the increase of adhesive strips. In the stage of tile leveling, the decline and fluctuation of contact area S_1 diminish with more adhesive strips, while the contact areas S_2 all remain constant. After the removal of shear vibration with compression, all the contact areas keep unchanged, except for the contact area S_1 under 13 strips which decreases slightly. At the end of unloaded stage, the contact areas S_1 and S_2 respectively increase by 5.35% and 0.67% with the increase of adhesive strips from 13 trips to 45 trips.

As mentioned above, the increase of adhesive strips causes narrower spacing between the adhesive strips. Consequently, more adhesive contacts with the tile and concrete, causing earlier rises of the contact areas S_1 and S_2. At the same time, there is a shorter distance from the outer adhesive strip to the edge of tile. This indicates that more adhesive is squeezed out of the tile under compression, increasing the $S_{1,\,max}$ and $S_{2,\,max}$ which ensures a bit more effects of shear vibration on the adhesive deformation. With respect to the diminished decline and fluctuation of contact area S_1, it is attributed to the more uniform deformation of adhesive under smaller amplitude of compression with the increase of adhesive strips. Due to the fact that the shear vibration acts at the tile-adhesive interface, all the contact areas S_2 remain stable. As mentioned in 4.2, the shear vibration induces the uniform plastic deformation of adhesive, ensuring most contact areas unchanged after the removal of loading. With respect to the slight decrease of contact area S_1 under 13 strips, it is attributed to the inhomogeneous adhesive deformation.

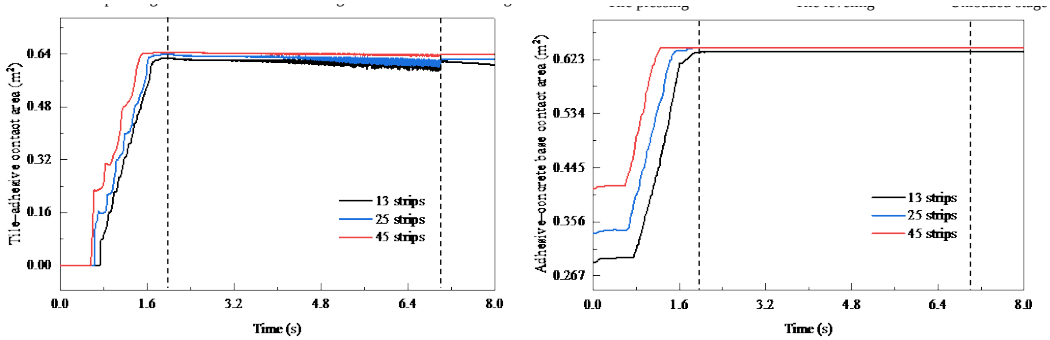

(a) Tile–adhesive contact area S_1 (b) Adhesive–concrete contact area S_2

Figure 12. Variations of the tile–adhesive contact area and adhesive–concrete contact area with time under various number of adhesive strips.

Figure 13 shows the distribution of interfacial defects under various number of adhesive strips. In the figure, the edge of tile is along the direction of adhesive application and the side of tile is perpendicular to the direction of adhesive application. It can be seen that with 13 adhesive strips, the tile-adhesive interfacial defect concentrates at the edge and distributes at the side, and the adhesive-concrete interfacial defect concentrates at the edge. These interfacial defects are provoked by inhomogeneous adhesive deformation. As the adhesive strips increase, more adhesive is squeezed to reach the edge of tile and more uniform deformation is produced in the adhesive. Thus, the increase of adhesive strips brings about the diminish of tile-adhesive interfacial defect into the shape of strips and the disappearance of adhesive-concrete interfacial defect as well as larger contact areas.

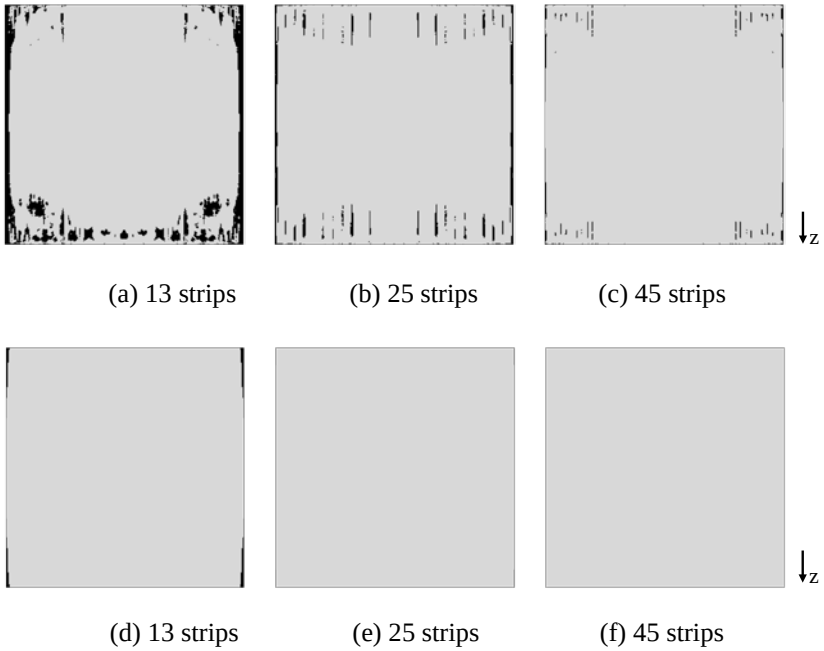

(a) 13 strips (b) 25 strips (c) 45 strips

(d) 13 strips (e) 25 strips (f) 45 strips

Figure 13. Contour plots of the distribution of interfacial defects under various number of adhesive strips. (a)-(c): tile-adhesive interfacial defects, (d-f): adhesive-concrete interfacial defects.

4.4 Effect of the yield stress of adhesive

At the initial moment of tile pressing, the deformation of adhesive with various yield stresses is shown in Figure14. Two indices including the height of adhesive strips and the spacing between adhesive strips were extracted to quantify the adhesive deformation. Obviously, the two indices ascend in a decreasing variation rate with higher yield stress of adhesive. Specifically, the variation rate of indices presents a large value at the low yield stresses smaller than 300 Pa. This is due to the fact that the adhesive strips produce large plastic deformation at the bottom once the yield stress of adhesive is lower than the stresses of adhesive induced by the gravity. As the yield stress of adhesive rises, the plastic deformation of adhesive decreases, and the shape of adhesive strips varies from semiellipse to circle. This can explain the ascends of the height of adhesive strips and the spacing between adhesive strips, which is respectively beneficial to a larger contact area S_1 and a better air discharge.

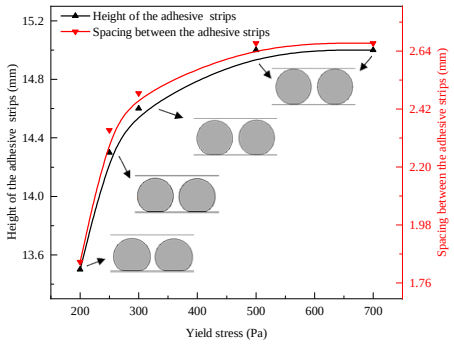

Figure 14. The deformation of adhesive with various yield stresses at the initial moment of tile pressing.

The effects of yield stress of adhesive on the rebounding value and vertical force of tile are exhibited in Figure 15. With the increase of yield stress of adhesive from 200 Pa to 700 Pa, the value of tile rebounding rises in an increasing variation rate. The maximum value F_m of pressing force at the end of tile pressing ascends from 2.15 kN to 7.42 kN, while the vertical force at the end of tile leveling changes from a pulling force of 0.11 kN to a pressing force of 2.42 kN.

As is well known, the adhesive produces less plastic deformation but more elastic deformation with higher yield stress. The increasing proportion of elastic deformation to the total deformation causes a larger total rebounding force, thereby increasing the maximum value F_m of pressing force. The decreasing proportion of plastic deformation to the total deformation indicates a smaller ratio of reduced rebounding force to the total rebounding force. Correspondingly, the vertical force at the end of tile leveling changes from a pulling force to a pressing force and the value of tile rebounding rises in an increasing variation rate.

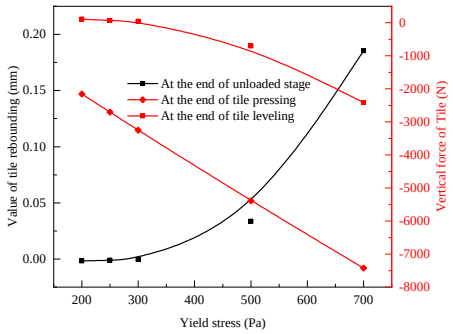

Figure 15. The rebounding value and vertical force of tile under various yield stress of adhesive.

Figure 16 presents the effect of yield stress of adhesive on the interfacial contact areas in the tiling system. As the yield stress of adhesive rises, the contact area S_1 decreases by 41.36% after a slight increase, and the contact area S_2 decreases slightly after a constant value of 0.64 m^2. Combined with the distribution of interfacial defects shown in Figure 17, the effect of yield stress of adhesive on the interfacial contact areas can be well interpreted. With low yield stress smaller than 300 Pa, the shear vibration causes large proportion of plastic deformation to the total deformation, especially at the edge and side of tile. Consequently, the adhesive detaches with the edge and side of tile but contacts well with the concrete. This can explain the slight increase of S_1 and constant S_2 before the yield stress of 300 Pa. As aforementioned, the growth of yield stress brings about a smaller ratio of reduced rebounding force to the total rebounding force. This indicates a less effect of shear vibration on the adhesive deformation, so the distributions of interfacial defects approximate more to the one under compression (Figure 10). That is, the contact areas S_1 and S_2 decline with the increase of yield stress after 300 Pa.

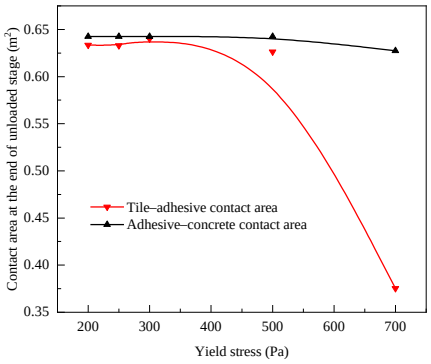

Figure 16. The interfacial contact areas in the tiling system under various yield stress of adhesive.

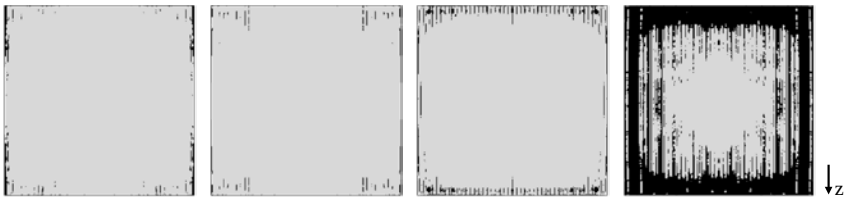

(a) 200 Pa (b) 300 Pa (c) 500 Pa (d) 700 Pa

(e) 200 Pa (f) 300 Pa (g) 500 Pa (h) 700 Pa

Figure 17. Contour plots of the distribution of interfacial defects under various yield stress of adhesive. (a)-(d): tile-adhesive interfacial defects, (e-h): adhesive-concrete interfacial defects.

5 Conclusions

In this study, the initial quality of robotic tile installation was investigated by establishing the fluid–structure coupling construction models of a tile–adhesive–concrete system. Based on these models, the influence laws and mechanisms of the pattern of adhesive application, the type of tile leveling loads, the number of adhesive strips and the yield stress of adhesive on the initial installation quality were discussed in depth. According to the results above, the following conclusions can be drawn.

- The adhesive strips after vertical application collapse with a semi-cylindrical shape and the spacing between them decreases because of the large equivalent plastic strains up to 4.16. By contrast, the adhesive after horizontal application produces small plastic deformation, causing the stable quasi-cylindrical shape of adhesive strips with evenly spaced distribution.
- Compared with a single compression load, its coupling with vertical vibration decreases the rebounding value of tile by 27.33% and the tile–adhesive contact area by 9.43%.

The inhomogeneous plastic deformation of adhesive is provoked by the vertical vibration, increasing the tile-adhesive interfacial defect with more concentration at the rim of tile. By contrast, the coupling of shear vibration with compression is beneficial to the avoidance of tile rebounding and the remarkable increase of the tile–adhesive contact area by 135.85%. The shear vibration boots the production of homogenous plastic deformation of adhesive, which ensures almost no interfacial defects.

- Increasing number of adhesive strips exerts few effects on the initial quality of robotic tile installation. As the number of adhesive strips increase, the shear vibration shows a bit more effects on the decrease of rebounding force of adhesive, thereby causing the transition of tile from the state of negligible rebounding to the one of negligible sinking. Additionally, a bit more adhesive is squeezed to reach the edge of tile and more homogenous deformation is produced in the adhesive. Thus, the increase of adhesive strips leads to slight increases of contact areas and diminished interfacial defects.
- Moderate yield stress of adhesive is essential for the high quality of tile installation. With low yield stress smaller than 300 Pa, the height of adhesive strips and the spacing between adhesive strips decreases drastically. The shear vibration causes large proportion of plastic deformation to the total deformation of adhesive as well as small rebounding force of adhesive and detachment of adhesive with the edge and side of tile, thereby provoking the sinking of tile and decrease of contact area S_1. With the growth of yield stress higher than 300 Pa, the shear vibration shows less effect on the adhesive deformation, which causes larger rebounding value of tile, decreased contact areas, and more approximate distributions of interfacial defects to the one under compression.

References

[1] Li, P., Li, Z., Yi, T., and Xi, G. (2018). *The application and development of building robot*, Machine Design and Research, 34(06), 25-29.

[2] Liu, T., Zhou, H., Xu, H., Du, Y. and Zhao, J. (2019). *Analysis of key points in automated installation technology of ceramic tile using robots*, Construction and Architecture, (11), 73-74.

[3] Gramazio, F. (2014). *Mobile Robotic Tiling*. [EB/OL]. https://fcl.ethz.ch/research/research-projects/mobile-robotic-tiling.html

[4] Apostolopoulos, D., Schempf, H. and West, J. (1996). *Mobile robot for automatic installation of floor tiles*. Proceedings of IEEE International Conference on Robotics and Automation, 22-28 April 1996, Minneapolis, MN, USA.

[5] Navon, R. (2000). *Process and quality control with a video camera, for a floor-tilling robot*, Automation in construction, 10(1), 113-125.

[6] Liu, H., Song, W. (2002). *An automatic robotic system for sticking ceramic tiles*, Robot Technique and Application, (04), 32-33.

[7] Liu, K. (2021). *Design and research of a new type paving robot*, Wuxi: Jiangnan University.

[8] Li, X., Sun C.H., Cheng W.L, Jiang X., and Liu Y.H. (2019). *Adaptive vision-based control for robotic tiling with uncalibrated cameras and limited FOV*. 2019 IEEE 15th International Conference on Control and Automation (ICCA), 16-19 July 2019, Edinburgh, UK.

[9] Wang S., Zhou H.X., Zhang Z.Y., Zheng X.Y., and Lv Y.N. (2021). *Robot floor-tiling control method based on finite-state machine and visual measurement in limited FOV*, Advances in Civil Engineering, 2021, 1–16.

[10] Xu S.B. (2020). *Design and performance test of automatic ceramic tile applicator*. Changsha: Central South University of Forestry and Technology.

[11] Noh, W.F. (1963). *CEL: A time-dependent, two-space-dimensional, Coupled Eulerian-Lagrange code*. United States.

[12] Benson, D.J. and Okazawa, S. (2004). *Contact in a multi-material Eulerian finite element formulation*, Computer methods in applied mechanics and engineering, 193(39-41), 4277-4298.